

Electrodynamics of a Magnet Moving through a Metallic Pipe

M. Hossein Partovi* and Eliza J. Morris†

Department of Physics and Astronomy, California State University, Sacramento, California 95819-6041

(Dated: December 24, 2018)

The popular demonstration involving a permanent magnet falling through a metallic pipe is treated as an azimuthally symmetric boundary value problem. Specifically, Maxwell's equations are solved for a uniformly magnetized, cylindrical bar magnet moving coaxially inside an infinitely long, conducting cylindrical shell of finite thickness at nonrelativistic speeds. Analytic solutions for the fields are developed and used to derive the resulting drag force acting on the magnet in integral form. This treatment provides a significant improvement over the existing ones, and can be made the basis of a quantitative laboratory experiment. A detailed analytical and numerical study of the properties of the drag force is presented. While the analysis is rigorous and the results are new, the presentation is primarily pedagogical and emphasizes clarity, completeness, and accessibility. Accordingly, extended discussions of approximations, estimation of neglected contributions, electrodynamics of moving magnets, material properties of the pipe, effect of the shape and speed of the magnet, and the role of energy conservation are presented.

PACS numbers: 03.65.Ud, 03.67.-a, 03.65.-w

I. INTRODUCTION

A. Background and Significance

A popular physics demonstration involves a permanent magnet falling through a metallic pipe^{1,2,3,4}. This arrangement has long been a favorite for demonstrating such topics as Faraday's law of induction, Lenz's law, eddy currents, inductive heating and magnetic damping. The underlying physical process is induction heating: the moving magnet creates a changing magnetic flux in its vicinity which induces circulating eddy currents within the pipe wall, thereby causing ohmic dissipation and generating a drag force on the magnet by energy conservation. The force itself is of course manifested as the action of the magnetic field generated by the eddies on the permanent magnet, with its retarding nature understood as a manifestation of Lenz's law. A particularly vivid picture of this mechanism emerges if one views the magnet as an assembly of circulating atomic currents moving through the pipe. Lenz's law then implies that the induced eddies in the pipe wall counter-circulate ahead of the moving magnet and co-circulate behind it. But this implies that the moving magnet is repelled in front and attracted in rear, hence acted upon by a retarding force.

An early contribution to the literature on this demonstration is Clack and Toepker,¹ who presented a description of the experiment and provided some measured results. Subsequently, Saslow² treated the problem of eddy currents in thin conducting sheets quite generally, and as an example provided an approximate calculation of the drag force on a magnet falling inside a conducting pipe. MacLatchy *et al.*³ used other methods to derive Saslow's result for the terminal speed and pointed out a sizable discrepancy between the predictions of this result and their measured values. These authors also developed a numerical simulation of the magnetic field inside the pipe that improved the agreement considerably. Hahn *et al.*⁴ considered a magnet undergoing an oscillatory motion inside the pipe, treating the damping force à la Saslow and MacLatchy augmented by some corrections for the finite length and thickness of the pipe (see the discussion below), and presented a comparison of their measured and predicted results. It is worth mentioning here that there is also a lively literature on the subject of magnetic braking in general that has a bearing on the present discussion⁵.

Following Saslow's calculation,² analytical treatments of the magnet-pipe problem have considered the magnet as a point dipole moving at low speeds and the pipe as infinitely thin-walled and long. These assumptions imply that the only significant length parameter in the problem is the interior diameter of the pipe, and lead to a simple expression for the drag force. We will refer to this limit as the *idealized model* and derive it as a limiting case of our general solution in Sec. [VB2](#). The point-dipole assumption corresponds to a magnet whose dimensions are negligible compared to the pipe diameter while being of sufficient strength. This assumption is not really justified for typical magnet-pipe parameters as MacLatchy *et al.*³ pointed out and as the results of our analysis in Sec. [VA](#) will demonstrate. The thin-wall assumption, on the other hand, requires the pipe thickness to be negligible compared to the radius of the pipe. In the experiments of MacLatchy *et al.* the pipe thickness was about 9% of its radius, not entirely negligible if quantitative agreement with observed data at a few percent level or better is desired. The restriction to small speeds, on the other hand, is moderately well satisfied for the typical arrangement where the magnet starts to fall through the pipe with zero initial velocity², as our discussion in Sec. [VA2](#) will confirm. On the other hand, the long-pipe

assumption is well satisfied as long as the magnet is not close to the ends of the pipe.

In summary, the idealized model fails to give a satisfactory quantitative agreement with experiment for a typical arrangement.^{3,4} The primary sources of inaccuracy in the model are the point-dipole and thin-wall assumptions, with the low-speed approximation a potential source of inaccuracy as well. These assertions will be quantitatively confirmed in Section V where we consider various approximations and limiting cases and compare them to the exact solution developed here.

B. Objectives and Limitations

Our objective in this work is to develop a formulation of the magnet-pipe system that is sufficiently realistic to yield an accurate prediction of the drag force at a few percent level or better. Specifically we will avoid the point-dipole and thin-wall assumptions of the idealized model, and instead treat the case of a uniformly magnetized, azimuthally symmetric, bar magnet moving coaxially inside an infinitely long, conducting cylindrical shell of arbitrary thickness. Since any practical realization of this model will likely involve magnet speeds far smaller than the speed of light, we will restrict our treatment to nonrelativistic speeds, $v/c \ll 1$, where v is the magnet speed and c is the speed of light. On the other hand, we are including the possibility of the magnet being projected into the pipe thus allowing much higher speeds than can be attained by a magnet that starts to fall from rest under gravity. The restriction to nonrelativistic speeds implies that we are dealing with quasi-static sources and fields where displacement currents can be neglected.⁶ This is so not only in the interior of the pipe where the inclusion of the displacement currents would amount to a minute correction of the order of $(v/c)^2$ but also within the pipe wall where conduction currents dominate displacement currents. To provide a basis for the latter assertion, we note that the basic time scale generated by the motion of the magnet is of the order of R_1/v , where R_1 is the inner radius of the pipe. This time scale corresponds to a frequency of the order of v/R_1 , which implies that the ratio of displacement to conduction currents is of the order of $\epsilon_0 v / \sigma R_1$ where σ is the conductivity of the pipe wall⁷. For common metals and with $1 \leq R_1 \leq 10$ cm, this ratio is in the $3(10^{-7} - 10^{-10})v/c$ range. Since $v/c \ll 1$ by assumption, the ratio in question is seen to be vanishingly small.

The assumption of an infinitely long pipe is unavoidable if a manageable solution is desired. The error resulting from this assumption, on the other hand, is small if the magnet is not close to the pipe ends. To provide a basis for this assertion, one can use the idealized solution, Sec. VB 2, to estimate the dissipated power within the pipe segment that extends from its actual end to its idealized end (which is infinitely far). The ratio of this quantity to the total dissipated power is then an estimate of the leading finite-length correction to the drag force. This ratio is found to be of the order of $(R_1/D)^7$, where D is the distance from the magnet to the near end of the pipe and R_1 is the pipe's interior diameter. For $R_1/D \lesssim 1/4$, for example, the expected correction would be of order 10^{-4} which is quite small as claimed.

Another approximation discussed above, namely the neglect of displacement currents, implies that the radiated power from the magnet-pipe assembly is negligible. Inasmuch as the motion of the magnet is accelerated before it reaches terminal speed, one would expect the magnet-pipe system to emit some electromagnetic radiation. To get an idea of the magnitude of such radiation, in Sec. II C we consider a permanent magnet possessing a magnetic dipole moment \mathbf{m} moving longitudinally (i.e., parallel to \mathbf{m}) through free space at nonrelativistic speeds. The radiated power from such a source, given in Eq. (13), is found to be $\mu_0 m^2 \ddot{v}^2 / 30\pi c^5$ where \dot{v} and \ddot{v} are the first and second time derivatives of the magnet's speed. This quantity should be compared to the ohmic dissipation in the pipe wall which for this purpose may be estimated using the idealized model. Using the solution to the idealized model given in Sec. VB 2, we estimate the ohmic dissipation rate to be $45\mu_0^2 m^2 v^2 \sigma s / 1024 R_1^4$ where s is the thickness of the pipe wall. For reasonable values of the parameters, the radiated power is totally dominated by the ohmic dissipation rate hence confirming the expectation that radiation is completely negligible in this problem.

This completes the discussion of the validity of various assumptions made in our formulation. While the analysis presented in this paper is rigorous and the results are new, the presentation is primarily pedagogical and emphasizes clarity, completeness, and accessibility. Accordingly such topics as the limits of validity of the existing results, the importance of neglected contributions, transformation properties of the magnet source currents, radiation emitted by a moving magnet, the role of energy conservation, and the effect on the drag force of the magnet shape and speed as well as the pipe conductivity and susceptibility are analyzed and discussed. These discussions extend beyond what is needed for a quantitative description of the magnet-pipe experiment. As we hope to demonstrate in this paper, the magnet-pipe system is a rich landscape of concepts and methods in electromagnetic theory, a fact that allows us to deal with several important physical phenomena in a concrete manner. Throughout we have strived to illustrate the importance of interweaving physical reasoning with mathematical techniques in analyzing physical problems.

The analytical and numerical results reported here, supplemented with a computer program posted on the web,⁸ can be made the basis of a quantitative laboratory experiment involving various aspects of the magnet-pipe system. Furthermore, certain aspects of the analysis or extensions thereof such as the asymptotic limits presented in Sec. VB

as well as others not treated here can be utilized as challenging assignments in mathematical methods.

The rest of this paper is organized as follows. Sec. II A deals with the characterization of the source currents of a permanent cylindrical magnet in axial motion at arbitrary speed, and II B with the vector potential of such a magnet in the quasi-static limit. The electromagnetic fields of the magnet-pipe system are found in Sec. III and the magnetic drag force is calculated in Sec. IV. Sec. V A presents the results of numerical computations for the drag force as well as a detailed discussion of its dependence on magnet shape and speed, and also on the material properties of the pipe. Several limiting cases of this dependence are explicitly verified in V B in the form of asymptotic formulas. Concluding remarks are presented in Sec. VI.

II. SOURCES AND FIELDS OF A MAGNET MOVING IN FREE SPACE

The first step in our analysis is the calculation of the electromagnetic fields of a permanent cylindrical magnet moving along its axis of symmetry in free space. We need these fields as input for the magnet-pipe configuration as well as for calculating the radiated power from a moving magnet, both for nonrelativistic motion. However, we begin our formulation under the more general conditions of arbitrary speed and acceleration, then specialize to nonrelativistic motion in order to derive the specific results needed for the magnet-pipe problem.

A. Source currents of a moving magnet

By a permanent (or *hard*) magnet is meant a ferromagnetic material whose magnetization does not change when immersed in external fields, electromagnetic or gravitational. In practice, this requirement is met for moderate electromagnetic or gravitational fields. Since the physical effects of acceleration are locally indistinguishable from those of gravity according to the equivalence principle,⁹ we conclude that a permanent magnet is unaffected by (moderate) acceleration. This conclusion allows us to characterize the accelerating magnet by means of equivalent sources in a reference frame \mathcal{S}' (with cylindrical space coordinates ρ', ϕ', z') in which it is instantaneously at rest, then transform this to the laboratory frame \mathcal{S} (with coordinates ρ, ϕ, z). In the laboratory frame then, the origin of \mathcal{S}' is specified by the coordinates $[0, 0, z_M(t)]$, where $z_M(t)$ is the z-coordinate of the center of mass of the magnet and $\dot{z}_M(t)\hat{\mathbf{z}}$ its velocity. Here and throughout, a caret denotes a unit vector.

The magnetization density of a cylinder of radius a and length L uniformly magnetized along its axis of symmetry can be represented by

$$\mathcal{M}'(\rho', z') = \frac{m}{\pi a^2 L} \Theta \left[\left(\frac{L}{2} \right)^2 - z'^2 \right] \Theta(a - \rho') \hat{\mathbf{z}} \quad (1)$$

in its instantaneous rest frame \mathcal{S}' . Here \mathcal{M}' is the magnetization density, $m\hat{\mathbf{z}}$ is the rest-frame magnetic dipole moment, and Θ is the standard step function. It is important to realize that in general the magnet is in accelerated motion, so that Eq. (1) embodies the stipulation that the magnetization of a permanent magnet is unaffected by acceleration.

Recall that the effective (or “bound”) current density,¹⁰ \mathbf{J}_M , is defined to be the source distribution equivalent to a given magnetization, i.e., $\mathbf{J}_M = \nabla \times \mathcal{M}$. Therefore, we have

$$\mathbf{J}'_M(\rho', \phi', z') = \frac{m}{\pi a^2 L} \Theta \left[\left(\frac{L}{2} \right)^2 - z'^2 \right] \delta(a - \rho') \hat{\phi}' \quad (2)$$

in the rest frame of the magnet. Observe that this current distribution is exactly that of an ideally wound solenoid of radius a and length L with a current per unit length of $m/(\pi a^2 L)$, as expected. This quantity must now be transformed to the laboratory frame.

At this juncture we recall that the charge and current density together transform as a 4-vector under a Lorenz transformation.¹¹ Here the charge density of the magnet vanishes in its rest frame, and since the current density vector is transverse with respect to the direction of relative motion, the charge density in the laboratory frame must vanish as well. As a result the transformation equations reduce to the simple result that $\mathbf{J}_M(\rho, \phi, z, t) = \mathbf{J}'_M(\rho', \phi', z')$. Note the emergence of the time dependence in $\mathbf{J}_M(\rho, \phi, z, t)$, which originates in the fact that z' depends on time as well as on z , as seen below.

The coordinates transform in the standard way: $\rho = \rho'$, $\phi = \phi'$, and $z' = \gamma[z - z_M(t)]$, where $\gamma = [1 - v^2/c^2]^{-1/2}$ and $v = \dot{z}_M(t)$. Note that we have suppressed the time dependence of v for brevity. Using the above relations, we

arrive at the result

$$\mathbf{J}_M(\rho, \phi, z, t) = \frac{m}{\pi a^2 L} \Theta \left\{ \left(\frac{L}{2} \right)^2 - \gamma^2 [z - z_M(t)]^2 \right\} \delta(a - \rho) \hat{\phi}, \quad (3)$$

which expresses the effective current density of the magnet in the laboratory frame \mathcal{S} . It is instructive to rewrite this in the slightly different form

$$\mathbf{J}_M(\rho, \phi, z, t) = \frac{m^{lab}}{\pi a^2 L^{lab}} \Theta \left\{ \left(\frac{L^{lab}}{2} \right)^2 - [z - z_M(t)]^2 \right\} \delta(a - \rho) \hat{\phi}, \quad (4)$$

where $L^{lab} = L/\gamma$ and $m^{lab} = m/\gamma$. Here the superscript “lab” refers to quantities as measured in the laboratory frame. Compared to the corresponding form in the rest frame, Eq. (2), this result indicates that the moving magnet undergoes length contraction as well as a contraction of magnetic dipole moment. The latter of course reflects time dilation, which causes a contraction of all currents in the magnet. The two effects leave the “current per unit length” of the equivalent solenoid invariant. For a sufficiently long magnet, this implies that the resultant magnetic field in the interior of the magnet is equal to $\hat{\mathbf{z}}\mu_0 m/(\pi a^2 L)$ in either reference frame¹². This is of course the familiar result that a magnetic field component parallel to the relative velocity does not change under Lorenz transformation. Similarly, one can readily show that the contraction of magnetic dipole moment found above is consistent with the known transformation properties of polarization and magnetization vectors.¹¹

B. Vector Potential of the Moving Magnet

Our task here is the calculation of the vector potential corresponding to the current density distribution of the moving magnet given in Eq. (4) in the quasi-static limit where displacement currents are neglected. Since in the case of the moving magnet the current density is transverse (or divergenceless) and the charge density vanishes, the Lorenz and Coulomb gauges are equivalent, with the common gauge condition given by $\nabla \cdot \mathbf{A}_M = 0$, where \mathbf{A}_M is the vector potential of the moving magnet. The electromagnetic fields of the magnet are of course obtained from the general relations $\mathbf{B} = \nabla \times \mathbf{A}$ and $\mathbf{E} = -\partial \mathbf{A}/\partial t$. The azimuthal symmetry of the current density, on the other hand, allows one to write $\mathbf{A}_M(\rho, \phi, z, t) = A_M(\rho, z, t) \hat{\phi}$. Thus the vector potential has an azimuthal ($\hat{\phi}$) component only which does not depend on the azimuthal coordinate ϕ , just like the current density vector. This implies that (a) the electric field is also purely azimuthal, and (b) the magnetic field has a radial ($\hat{\rho}$) as well as a longitudinal ($\hat{\mathbf{z}}$) component. It is of course the former component that exerts the retarding force on the moving magnet.

Using the standard solution for the vector potential in the quasi-static limit, we find

$$A_M^{qs}(\rho, z, t) = \frac{\mu_0}{4\pi} \int dz' d\phi' \rho' d\rho' [\rho^2 + \rho'^2 - 2\rho\rho' \cos(\phi - \phi') + (z - z')^2]^{-\frac{1}{2}} \times J_M^{qs}(\rho', z', t) \cos(\phi - \phi'), \quad (5)$$

where we have used $\hat{\phi} \cdot \hat{\phi}' = \cos(\phi - \phi')$. Here “qs” is a reminder that the quantity in question is being evaluated in the quasi-static limit.¹³ In particular, J_M^{qs} is obtained from Eq. (4) by setting $\gamma = 1$. Making this substitution, then, we find

$$A_M^{qs}(\rho, z, t) = \frac{m}{\pi a L} \frac{\mu_0}{4\pi} \int dz' d\phi' [\rho^2 + a^2 - 2\rho a \cos(\phi - \phi') + (z - z')^2]^{-\frac{1}{2}} \times \Theta \left\{ \left(\frac{L}{2} \right)^2 - [z' - z_M(t)]^2 \right\} \cos(\phi - \phi'), \quad (6)$$

where we have already carried out the integration over the radial coordinate.

To facilitate the remaining integrations in Eq. (6), we make use of the following representation which is valid for $\rho \geq a$:¹⁴

$$[\rho^2 + a^2 - 2\rho a \cos(\phi - \phi') + (z - z')^2]^{-\frac{1}{2}} = \frac{2}{\pi} \int_{-\infty}^{+\infty} dk \exp[ik(z - z')] \times \left\{ \frac{1}{2} I_0(\sqrt{k^2} a) K_0(\sqrt{k^2} \rho) + \sum_{n=1}^{\infty} \cos[n(\phi - \phi')] I_n(\sqrt{k^2} a) K_n(\sqrt{k^2} \rho) \right\}, \quad (7)$$

where I_n and K_n are modified Bessel functions of the first and second kind of order n , respectively. Here and below we will use $\sqrt{\xi}$ to denote that root of ξ which has a positive real part when ξ does. Of course when ξ is real and positive, this notation reduces to the standard convention whereby $\sqrt{\xi}$ stands for the positive root of ξ . Note also that for $0 \leq \rho \leq a$, a and ρ must be interchanged in Eq. (7).

Using the representation of Eq. (7) in Eq. (6), we find

$$A_M^{qs}(\rho, z, t) = \frac{m\mu_0}{2a\pi^2} \int_{-\infty}^{+\infty} dk \exp\{ik[z - z_M(t)]\} \frac{\sin(kL/2)}{(kL/2)} I_1(|k|a) K_1(|k|\rho), \quad (8)$$

which is valid for $\rho \geq a$. It is worth mentioning that this result can also be viewed as the magnetostatic potential of a (longitudinally moving) solenoid of radius a , length L , and current per unit length of $m/(\pi a^2 L)$.

C. Radiation by an Accelerated Magnet

A second result to be derived from Eq. (4) is the power radiated by the moving magnet in the nonrelativistic limit $v \ll c$. This radiation involves the fields of the magnet in the *far zone*.¹⁵ These *radiation fields* are conveniently calculated by considering the retarded solution arising from the source currents of Eq. (4) in a general form:

$$\mathbf{A}_M(\mathbf{r}, t) = \frac{\mu_0}{4\pi} \int d^3 \mathbf{r}' |\mathbf{r} - \mathbf{r}'|^{-1} \mathbf{J}_M(\mathbf{r}', t_{ret}), \quad (9)$$

where \mathbf{r}' and \mathbf{r} locate the source and field points, respectively, and $t_{ret} = t - |\mathbf{r} - \mathbf{r}'|/c$. The radiation fields are obtained from Eq. (9) as its leading contribution in the limit $|\mathbf{r}'|/|\mathbf{r}| \rightarrow 0$:

$$\mathbf{A}_M^{rad}(\mathbf{r}, t) = \frac{\mu_0}{\pi |\mathbf{r}|} \int d^3 \mathbf{r}' \mathbf{J}_M(\mathbf{r}', t - \frac{r}{c} - \frac{\hat{\mathbf{r}} \cdot \mathbf{r}'}{c}), \quad (10)$$

where we have used the radiation zone condition $|\mathbf{r} - \mathbf{r}'| \rightarrow |\mathbf{r}| - \hat{\mathbf{r}} \cdot \mathbf{r}'$.

Next we consider the nonrelativistic limit, which allows us to expand \mathbf{J}_M in the quantity $\hat{\mathbf{r}} \cdot \mathbf{r}'/c$ and let $\gamma \rightarrow 1$. The zeroth-order term in the expansion vanishes because \mathbf{J}_M is divergenceless. The first-order contribution, corresponding to the magnetic dipole radiation, is static and gives a vanishing electric field as $\gamma \rightarrow 1$.¹⁶ The second order term, corresponding to magnetic quadrupole radiation, survives and is the leading contribution:

$$\mathbf{A}_M^{rad, NR}(\mathbf{r}, t) = \frac{\mu_0}{4\pi |\mathbf{r}|} \int d^3 \mathbf{r}' \ddot{\mathbf{J}}_M^{NR}(\mathbf{r}', t - \frac{r}{c}) \frac{1}{2} \left[\frac{\mathbf{r} \cdot \mathbf{r}'}{c|\mathbf{r}|} \right]^2, \quad (11)$$

where “NR” indicates the nonrelativistic limit and a dot signifies differentiation with respect to the time argument. At this point we substitute the expression for \mathbf{J} from Eq. (4), set $\gamma = 1$, and perform the integration and other implied operations in Eq. (11). The result is

$$\mathbf{A}_M^{rad, NR}(\mathbf{r}, t) = \frac{\mu_0 m}{8\pi r c^2} \sin(2\theta) \ddot{z}_M(t - \frac{r}{c}) \hat{\phi}, \quad (12)$$

where θ is the polar angle defined by $\cos(\theta) = \hat{\mathbf{z}} \cdot \hat{\mathbf{r}}$ and $\ddot{z}_M = \ddot{v}$. The radiation fields of the magnet can now be found from Eq. (12) using $\mathbf{E}^{rad} = -\dot{\mathbf{A}}_M^{rad, NR}$ and $\mathbf{B}^{rad} = \hat{\mathbf{r}} \times \mathbf{E}^{rad}/c$.

It is now a matter of standard procedure to find the radiated power by means of Poynting’s vector. The latter is given here by $\mathbf{S}^{rad} = |\dot{\mathbf{A}}_M^{rad, NR}|^2 \hat{\mathbf{r}}/\mu_0 c$, and has the four-pronged angular distribution $\sim \sin(2\theta)^2$ characteristic of quadrupole radiation. Finally the total radiated power is found by integrating $\hat{\mathbf{r}} \cdot \mathbf{S}^{rad}$ over the surface of a large sphere, with the result

$$P^{rad} = \frac{\mu_0 m^2 \ddot{v}^2}{30\pi c^5}. \quad (13)$$

Note that the radiated power does not depend on the shape of the magnet so that Eq. (13) holds in the point-dipole limit as well. Note also that the radiated power is proportional to \ddot{v}^2 and will vanish for a uniformly accelerating magnet.

III. ELECTROMAGNETIC FIELDS OF THE MAGNET-PIPE SYSTEM

Having developed the near and far fields of the moving magnet in free space, we now turn to finding the fields of the magnet-pipe system. We do this by developing the general solution first, followed by the imposition of continuity conditions.

A. General Solution

Our first task here is finding the governing equations for the vector potential in the three regions (i) $a \leq \rho \leq R_1$, (ii) $R_1 \leq \rho \leq R_2$, and (iii) $R_2 \leq \rho$, where R_1 and R_2 are the inner and outer radii of the pipe, respectively.¹⁷ We will actually treat the case of a medium with permeability μ and conductivity σ corresponding to region (ii). For regions (i) and (iii), we will simply replace these with μ_0 and 0, respectively. Recall from our discussion in the Sec. I B that the fields of the magnet-pipe system can be safely calculated in the quasi-static limit where displacement currents are neglected. Therefore the equation obeyed by the vector potential in the Lorenz (or radiation) gauge reduces to

$$(\nabla^2 - \mu\sigma\partial/\partial t)\mathbf{A} = 0. \quad (14)$$

As we saw in Sec. II B, the azimuthal symmetry of the system allows us to represent the vector potential in the form $\mathbf{A}(\rho, \phi, z, t) = A(\rho, z, t)\hat{\phi}$. Moreover, $A(\rho, z, t)$ is conveniently represented as a Fourier integral following the example of Eq. (8):

$$A(\rho, z, t) = (2\pi)^{-1/2} \int_{-\infty}^{+\infty} dk \exp\{ik[z - z_M(t)]\} \tilde{A}(\rho, k). \quad (15)$$

The inverse transformation is given by

$$\tilde{A}(\rho, k) = (2\pi)^{-1/2} \int_{-\infty}^{+\infty} dz \exp\{-ik[z - z_M(t)]\} A(\rho, z, t). \quad (16)$$

Using this representation in Eq. (14), we find

$$\left(\frac{\partial^2}{\partial \rho^2} + \frac{1}{\rho} \frac{\partial}{\partial \rho} - \frac{1}{\rho^2} - k^2 + ik\mu\sigma v\right) \tilde{A}(\rho, k) = 0. \quad (17)$$

The general solution of Eq. (17) is a linear combination of $I_1(\sqrt{\kappa^2}\rho)$ and $K_1(\sqrt{\kappa^2}\rho)$, where $\kappa^2 = k^2 - i\mu\sigma v k$.¹⁸ Recall that $\sqrt{\kappa^2}$ stands for that root of κ^2 which has a positive real part. Now $K_1(\sqrt{\kappa^2}\rho)$ is singular at $\rho = 0$ and vanishes exponentially as $\rho \rightarrow \infty$, while $I_1(\sqrt{\kappa^2}\rho)$ vanishes at $\rho = 0$ but diverges exponentially as $\rho \rightarrow \infty$. Using this information, we construct the solution to Eq. (17) in the three regions as follows:

$$\tilde{A}^{(i)}(\rho, k) = \tilde{A}_M^{qs}(\rho, k) + b_1 I_1(|k|\rho), \quad (18)$$

$$\tilde{A}^{(ii)}(\rho, k) = b_2 K_1(\sqrt{\kappa^2}\rho) + b_3 I_1(\sqrt{\kappa^2}\rho), \quad (19)$$

$$\tilde{A}^{(iii)}(\rho, k) = b_4 K_1(|k|\rho), \quad (20)$$

where $\tilde{A}_M^{qs}(\rho, k) = b_0 K_1(|k|\rho)$ is the term corresponding to the potential of the moving magnet. Comparing Eqs. (8) and (15), we find

$$b_0(k) = \frac{m\mu_0}{2a\pi^2} (2\pi)^{1/2} \frac{\sin(kL/2)}{(kL/2)} I_1(|k|a). \quad (21)$$

Above, $\tilde{A}^{(n)}(\rho, k)$ represents the solution to Eq. (17) in the n th region. Note that we have set $\sigma = 0$ for regions (i) and (iii) as stipulated.

Using the analogy of waves, one may interpret the terms appearing in Eqs. (18-20) as “reflections” and “transmissions” resulting from the “incident” term $\tilde{A}_M^{qs}(\rho, k)$. This source term representing the contribution of the moving magnet is incident upon the inner surface of the pipe. The second term in region (i) is the reflection from the inner surface of the pipe into the interior. The two terms in region (ii) correspond to a linear combination of the transmitted term from region (i) and the reflected term from the outer surface of the pipe. In region (iii) we only have the transmitted term from region (ii), since there will be no reflection from “the surface at infinity.” From a mathematical point of view, on the other hand, one starts with a linear combination of the solutions of Eq. (17) in each region and proceeds to impose the required boundary conditions. Thus in region (i), the singular term $[K_1(|k|\rho)$, singular at $\rho = 0$] is normalized to represent the contribution of the moving magnet, while in region (iii), the singular term $[I_1(|k|\rho)$, singular at $\rho = \infty$] is excluded to ensure that the fields vanish far from the magnet-pipe system. Of course the physical sources of all six terms are the (bound) magnetization currents in the magnet and in the pipe wall as well as the conduction currents in the pipe wall.

B. Continuity Conditions

Our next task is the formulation of continuity conditions across the two boundary surfaces, the inner and outer surfaces of the pipe wall. We recall from above that the electric field is purely azimuthal while the magnetic field has a radial as well as a longitudinal component. We will denote these E_ϕ ($= \hat{\phi} \cdot \mathbf{E}$), B_ρ ($= \hat{\rho} \cdot \mathbf{B}$), and B_z ($= \hat{\mathbf{z}} \cdot \mathbf{B}$), respectively. Now the boundary conditions require the continuity of E_ϕ (Faraday's law), B_ρ (absence of magnetic monopoles), and H_z (the Ampère-Maxwell law and absence of surface currents) across the two boundary surfaces, where $\mathbf{H} = \mathbf{B}/\mu_0$ in regions (i) and (iii), and $\mathbf{H} = \mathbf{B}/\mu$ in region (ii). When expressed in terms of \mathbf{A} , the first two of these conditions require the continuity of A while the third condition requires the continuity of $\mu^{-1}\partial(\rho A)/\partial\rho$. An inspection of Eq. (16) shows that these conditions must also be obeyed by \tilde{A} . This gives us the continuity equations that must be imposed on the solutions of Eq. (17). Recall that we must also apply the conditions $\kappa \rightarrow k$ and $\mu \rightarrow \mu_0$ in regions (i) and (iii).

Upon imposing the above-stated continuity conditions on the solutions given in Eqs. (18-20) at the boundary surfaces $\rho = R_1$ and $\rho = R_2$, we find the following set of equations:

$$\begin{aligned} b_0 K_1(|k|R_1) + b_1 I_1(|k|R_1) &= b_2 K_1(\sqrt{\kappa^2} R_1) + b_3 I_1(\sqrt{\kappa^2} R_1), \\ b_2 K_1(\sqrt{\kappa^2} R_2) + b_3 I_1(\sqrt{\kappa^2} R_2) &= b_4 K_1(|k|R_2), \\ \frac{|k|}{\mu_0} [-b_0 K_0(|k|R_1) + b_1 I_0(|k|R_1)] &= \frac{\sqrt{\kappa^2}}{\mu} [-b_2 K_0(\sqrt{\kappa^2} R_1) + b_3 I_0(\sqrt{\kappa^2} R_1)], \\ \frac{\sqrt{\kappa^2}}{\mu} [-b_2 K_0(\sqrt{\kappa^2} R_2)] + b_3 I_0(\sqrt{\kappa^2} R_2) &= \frac{|k|}{\mu_0} [-b_4 K_0(|k|R_2)]. \end{aligned} \quad (22)$$

This linear set can be solved by standard methods to find the unknown coefficients b_1 through b_4 . To avoid unnecessary writing, we will only record the solution for b_1 , since this is the coefficient that will be needed for the calculation of the drag force in Sec. V:

$$\begin{aligned} b_1(k) &= \{[K_0(|k|R_1)K_0(|k|R_2)T_{11} + \beta K_0(|k|R_1)K_1(|k|R_2)T_{10} \\ &\quad - \beta K_1(|k|R_1)K_0(|k|R_2)T_{01} - \beta^2 K_1(|k|R_1)K_1(|k|R_2)T_{00}] \\ &\quad \div [I_0(|k|R_1)K_0(|k|R_2)T_{11} + \beta I_0(|k|R_1)K_1(|k|R_2)T_{10} \\ &\quad + \beta I_1(|k|R_1)K_0(|k|R_2)T_{01} + \beta^2 I_1(|k|R_1)K_1(|k|R_2)T_{00}]\}b_0(k), \end{aligned} \quad (23)$$

where

$$\begin{aligned} T_{00} &= K_0(\alpha|k|R_1)I_0(\alpha|k|R_2) - I_0(\alpha|k|R_1)K_0(\alpha|k|R_2) \\ T_{01} &= K_0(\alpha|k|R_1)I_1(\alpha|k|R_2) + I_0(\alpha|k|R_1)K_1(\alpha|k|R_2) \\ T_{10} &= K_1(\alpha|k|R_1)I_0(\alpha|k|R_2) + I_1(\alpha|k|R_1)K_0(\alpha|k|R_2) \\ T_{11} &= K_1(\alpha|k|R_1)I_1(\alpha|k|R_2) - I_1(\alpha|k|R_1)K_1(\alpha|k|R_2), \end{aligned} \quad (24)$$

and

$$\begin{aligned} \alpha &= \sqrt{\kappa^2}/\sqrt{k^2} = \sqrt{1 - i\frac{\mu_0\mu_{rel}\sigma v}{k}}, \\ \beta &= \frac{\alpha}{\mu_{rel}} = \frac{1}{\mu_{rel}}\sqrt{1 - i\frac{\mu_0\mu_{rel}\sigma v}{k}}. \end{aligned} \quad (25)$$

Here $\mu_{rel} = \mu/\mu_0$ represents the relative permeability of the pipe material. It is worth noting that α and β have positive real parts by construction.

With the coefficients given in Eqs. (23-25), we have in Eqs. (15) and (18-21) a complete solution to the magnet-pipe system in all regions.

IV. DRAG FORCE ON THE MOVING MAGNET

We are now in position to calculate the braking force exerted by the magnetic field on the moving magnet. Recall that the density of magnetic force exerted at a point \mathbf{r} of a current distribution $\mathbf{J}(\mathbf{r})$ is given by $\mathbf{J}(\mathbf{r}) \times \mathbf{B}(\mathbf{r})$, where

$\mathbf{B}(\mathbf{r})$ is the magnetic field strength at the point in question. Thus the force exerted on the moving magnet is given by

$$\mathbf{F} = \int d^3(\mathbf{r}) \mathbf{J}_M(\mathbf{r}, t) \times \mathbf{B}(\mathbf{r}), \quad (26)$$

where $\mathbf{J}_M(\mathbf{r}, t)$ is the effective current density of the magnet given in Eq. (3) in the nonrelativistic limit $\gamma = 1$. Note that $\mathbf{B}(\mathbf{r})$ can be replaced with $\mathbf{B}^{ext}(\mathbf{r})$ in Eq. (26), where the latter is the magnetic field produced in region (i) by sources external to the magnet. Using Eqs. (15) and (18), we find

$$\mathbf{B}^{ext}(\mathbf{r}) = \nabla \times (2\pi)^{-1/2} \int_{-\infty}^{+\infty} dk \exp\{ik[z - z_M(t)]\} b_1(k) I_1(|k|\rho) \hat{\phi}. \quad (27)$$

Combining the above equations and performing a few straightforward operations, we find

$$\mathbf{F} = -\hat{\mathbf{z}} \frac{\mu_0 m^2}{4\pi^2} \int_{-\infty}^{+\infty} dk k^3 \left[\frac{\sin(kL/2)}{(kL/2)} \right]^2 \left[\frac{I_1(|k|a)}{(ka/2)} \right]^2 Q(k)/i, \quad (28)$$

where $Q(k) = b_1(k)/b_0(k)$ is implicit in Eqs. (23-25) *et seq.* An inspection of Eqs. (23-25) shows that the real and imaginary parts of $Q(k)$ are even and odd functions of k , respectively. Thus we can rewrite Eq. (28) in the form

$$\mathbf{F} = -\hat{\mathbf{v}} \frac{\mu_0 m^2}{4\pi^2} \int_0^{+\infty} dk k^3 \left[\frac{\sin(kL/2)}{(kL/2)} \right]^2 \left[\frac{I_1(ka)}{(ka/2)} \right]^2 2 \operatorname{Im}[Q(k)]. \quad (29)$$

This equation gives the drag force acting on the moving magnet and is a central result of our analysis.

It is instructive to rederive this result from the energy conservation principle. Let us consider the magnet-pipe system at a moment the magnet is moving through the pipe with velocity \mathbf{v} . Under the quasi-static conditions stipulated in the Sec. 1B, ohmic power dissipation in the pipe wall must be balanced by a matching decrease in the kinetic energy of the moving magnet, since the power flow into the electromagnetic field configuration, including radiation, is negligible. But the decrease in kinetic energy corresponds to a resistive force according to the work-energy theorem, $P_{ohm} = -\mathbf{F} \cdot \mathbf{v}$, where P_{ohm} is the rate of ohmic dissipation (or Joule heating). Needless to say, the magnet may be experiencing non-electromagnetic forces such as gravity or air drag which would have their own power contributions. Now Poynting's theorem assures us that the dissipated power equals the flux of Poynting's vector into the pipe wall through its inner surface. Putting these two observations together, we arrive at

$$\mathbf{F} \cdot \mathbf{v} = - \int_{\rho=R_1} \rho d\phi dz \mathbf{S} \cdot \hat{\rho}, \quad (30)$$

where \mathbf{S} is Poynting's vector, given by $= \mu_0^{-1} \mathbf{E} \times \mathbf{B}$. Since by symmetry \mathbf{F} must have an axial direction, we can rewrite Eq. (30) as

$$\mathbf{F} = -\hat{\mathbf{v}} \frac{1}{\mu_0 v} \int_{\rho=R_1} \rho d\phi dz \hat{\rho} \cdot \left[\frac{\partial \mathbf{A}}{\partial t} \times (\nabla \times \mathbf{A}) \right], \quad (31)$$

where we have used $\mathbf{B} = \nabla \times \mathbf{A}$ and $\mathbf{E} = -\partial \mathbf{A}/\partial t$.

At this juncture we use Eq. (15) to substitute the appropriate representation of A into Eq. (31). This allows us to perform all implied integrations except one, with the result

$$\mathbf{F} = -\hat{\mathbf{v}} \frac{\pi R_1}{\mu_0} \int_{-\infty}^{\infty} dk (-ik) \left[\frac{\partial [\tilde{A}^{(i)}(\rho, k)]^2}{\partial \rho} \right]_{\rho=R_1}. \quad (32)$$

Next, we use Eq. (18) to replace $\tilde{A}^{(i)}(\rho, k)$ with its expression in terms of modified Bessel functions. Of the resulting four terms inside the square brackets, two are even in k and make no contribution to the integral in Eq. (32). The other two terms equal $|k|b_0(k)b_1(k)W$, where $W = 1/|k|R_1$ is the Wronskian of K_1 and I_1 .¹⁸ Upon replacing $b_1(k)$ with $b_0(k)Q(k)$ in Eq. (32), and noting that $Q(k)$ is odd and pure imaginary, we recover Eq. (29). This completes the derivation of the magnetic drag force from energy conservation.

V. PROPERTIES OF THE DRAG FORCE

This section is devoted to a detailed discussion of the properties of the drag force derived above. We shall begin by characterizing the main features of the drag force in Sec. V A, including its dependence on the shape and speed of the magnet as well as the material properties of the pipe wall. We will then outline the derivation of asymptotic expressions for a number of useful limiting cases in Sec. V B.

A. Main Features

1. Dependence on Magnet Shape

Let us start by examining the dependence of the drag force on the dimensions of the magnet. We have already arranged Eq. (29) in such a way as to isolate and highlight the dependence of the drag force on the relevant parameters. The force is opposite the velocity¹⁹ and it is scaled by the square of the magnet's dipole moment.²⁰ For a fixed value of the dipole moment, the dependence of the force on the dimensions of the magnet is entirely contained in the two bracketed factors in Eq. (29), the first of which depends on the magnet length L and the second on its radius a . Each of these factors has been normalized to unity at the point-dipole limit, the first at $L = 0$ and the second at $a = 0$. An inspection of the second factor shows that it increases monotonically with increasing a , which is expected as such an increase brings the source currents in the magnet closer to the eddy currents in the pipe wall thus increasing the interaction force. On the other hand, the envelope of the first factor clearly decreases with increasing magnet length, suggesting a corresponding decrease in the drag force with increasing magnet length. This is in fact confirmed by our numerical results, and reflects the weakening of the external magnetic field with increasing magnet length (with a fixed magnetic dipole moment as stipulated), which field eventually vanishes as $L/a \rightarrow \infty$, just as it would for an ideal solenoid. It must be remembered, however, that a can at most equal R_1 , and L must remain small compared to the distance from the magnet to the pipe ends. It is convenient in this regard to define an ordered pair of dimensionless parameters, $(L/2a, a/R_1)$, characterizing the inverse aspect ratio of the magnet and the tightness of its fit inside the pipe, respectively. Thus for a given dipole strength, the pair $(0, 1.00)$ corresponds to a wafer-shaped magnet that would just fit inside the pipe while $(1, 0.60)$ describes a “square cylinder” filling 36% of the interior cross section of the pipe.

Numerical results were obtained from Eq. 29 using a *Mathematica* program developed for this purpose.⁸ Figure 1 shows a plot of the drag force versus magnet speed for $m = 1.00 \text{ A m}^2$, $\mu_{\text{rel}} = 1.00$, $\sigma = 5.00 \times 10^7 \Omega^{-1} \text{ m}^{-1}$, $R_1 = 10.0 \text{ mm}$, $R_2 = 11.0 \text{ mm}$, and five different shapes, (a) (typical cylinder, loose fit) $\Rightarrow (\frac{2}{1}, 0.60)$, (b) (“square” cylinder, loose fit) $\Rightarrow (\frac{1}{1}, 0.60)$, (c) point-like cylinder $\Rightarrow (\frac{1}{1}, \simeq 0)$, (d) (short cylinder, snug fit) $\Rightarrow (\frac{5}{8}, 0.96)$ (e) (circular wafer, loose fit) $\Rightarrow (\simeq 0, 0.60)$. The dashed line, on the other hand, represents the idealized model limit derived in Sec. V B 2, $\mathbf{F}^{\text{id}} = -\hat{\mathbf{v}}45\mu_0^2m^2v\sigma s/1024R_1^4$, with the pipe thickness s set equal to $R_2 - R_1 = 1.0 \text{ mm}$ in order to facilitate comparison to the exact results.

The five cases shown in Fig. 1 demonstrate the effect of the shape of the magnet on the drag force. A comparison of cases (a) and (b) in Fig. 1 clearly shows that for fixed values of the dipole moment and speed the drag force increases as the magnet is shortened. Comparing cases (b) and (d), or (c) and (e), on the other hand, we see an increase in the drag force with increasing magnet diameter. These five cases clearly demonstrate the strong influence of the shape of the magnet on the drag force. In particular, they clearly demonstrate the quantitative inadequacy of the point-dipole approximation, case (c), across a broad range of speeds, as discussed in Sec. I A.

The dashed line representing the idealized model corresponds to augmenting the point-dipole approximation by the thin-wall assumption, $(R_2 - R_1)/R_1 \rightarrow 0$.²¹ A comparison of the dashed line and curve (c) in Fig. 1 shows a relative deviation of about 10% in the low-speed regime. This deviation should be compared with the ratio $(R_2 - R_1)/R_1$ characterizing the relative thickness of the pipe, which equals 0.100 for all cases in Fig. 1. It is clear that the error caused by the thin-wall assumption is in general unacceptably large for a reasonable agreement with measurement results under typical conditions. Exceptions can of course occur: for case (d) corresponding to a short cylindrical magnet fitting snugly inside the pipe, the errors caused by the point-dipole and thin-wall approximations nearly cancel one another in the low-speed regime.

It is appropriate at this juncture to compare the prediction of our analysis to the measured results of MacLatchy *et al.*³. Using the parameter values reported by these authors, namely $m = 0.67 \text{ A m}^2$, $\sigma = 5.08 \times 10^7 \Omega^{-1} \text{ m}^{-1}$, $R_1 = 7.29 \text{ mm}$, $R_2 = 7.96 \text{ mm}$, $L = 6.4 \text{ mm}$, and $a = 6.3 \text{ mm}$, and equating their reported magnet (plus tape) weight of 0.060 N to the magnetic drag force of Eq. 29 as well as setting $\mu_{\text{rel}} = 1.00$ appropriate for copper, we find a magnet speed of $11.9 \pm 0.5 \text{ cm s}^{-1}$. MacLatchy *et al.* reported a measured terminal speed of $12.7 \pm 0.4 \text{ cm s}^{-1}$, and compared this to the prediction of the idealized model, 17.8 cm s^{-1} , and the result of their numerical model, 13.0 cm s^{-1} . Note

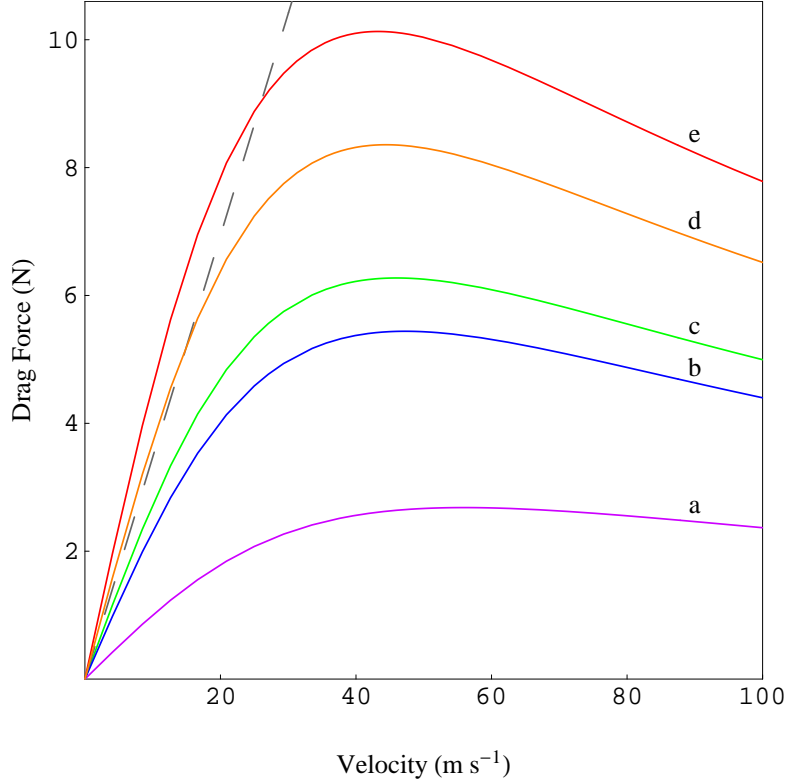


FIG. 1: Plot of the drag force versus the magnet speed for a fixed value of the dipole moment and four different shape parameters ($L/2a, a/R_1$) (see the text for definitions): (a) typical cylinder, $(\frac{2}{1}, 0.60)$, (b) “square” cylinder, $(\frac{1}{1}, 0.60)$, (c) “point-like cylinder” $(\frac{1}{1}, \simeq 0)$, (d) short cylinder $(\frac{5}{8}, 0.96)$, and (e) circular wafer, $(\simeq 0, \frac{3}{5})$. The dashed line represents the idealized limit.

that in this comparison we are neglecting the air drag force on the magnet, estimated by MacLatchy *et al.* to be less than 0.1% of the magnetic drag force hence deemed negligible. The quoted error of 0.5 cm s^{-1} in our calculated result is estimated on the basis of the (implied) precision level of the measured values given by MacLatchy *et al.* for $L, a, m, R_2 - R_1$, and the magnet weight. Keeping in mind that other sources of error such as the actual magnetization distribution of the magnet and the tendency of the magnet to wobble as it falls through the pipe are disregarded in the above error estimates, we conclude that our predicted value of the magnet speed agrees with the measured value within the error limits.

The circular wafer ($L = 0$) geometry merits special attention since in that case the drag force grows without limit as $a \rightarrow R_1$. In other words, the shape characterized by $(0, 1)$ is a singular limit where the magnetic drag force diverges. This behavior may be understood as follows. In the limit of $(0, 1)$ geometry, the effective (or “bound”) source currents of the magnet are concentrated in a single current ring of radius R_1 . However, such a source would induce similarly concentrated eddy current rings in the pipe wall on its interior surface, i.e., at zero distance from the source itself thus causing infinite interaction forces due to overlapping current rings. This situation is analogous to the divergence of the image force on a point charge as it approaches the surface of a conductor. It is worth remarking that while the limit itself is unphysical, the sharp increase in the magnetic drag force for $L \ll a$ and $a \rightarrow R_1$ is very real and already discernible from a comparison of cases (c) and (e) in Fig. 1. In practice, this sharp increase in the magnetic drag would be accompanied by a parallel increase in the air drag force caused by the unavoidable constriction in the flow of air around the magnet.²²

The effect just discussed can also be understood by reference to Eq. 29. Using the asymptotic properties of the modified Bessel functions,¹⁸ we find that $\text{Im}[Q(k)] \rightarrow \exp(-2kR_1)/k$ as $k \rightarrow \infty$. Now for $L/a \rightarrow 0$ and $a \rightarrow R_1$, the shape factors in Eq. (29) behave like $\exp(2kR_1)/k^3$ as $k \rightarrow \infty$. Putting these two statements together, we conclude that the integrand in Eq. (29) behaves like k^{-1} for large k , which implies a logarithmic divergence at the upper limit of the integral. Recalling that k is the Fourier conjugate of z [cf. Eq. (29)], so that large values of k are associated with short values of z , we conclude that this divergence is a short-distance effect. This is of course the conclusion we reached above on physical grounds.

2. Dependence on Magnet Speed

The dependence of the drag force on the speed of the magnet is contained in $Q(k)$ through the combination $\mu\sigma v$ and is more involved than the dependence on its shape. It proves expedient to discuss this dependence in terms of a length parameter defined by $l_0 = (\mu_0\sigma v)^{-1}$. As discussed below, l_0 represents the penetration depth of the fields into the pipe wall under appropriate conditions. The two distinguished ranges of v , which we will refer to as “low” and “high” speed,²³ correspond to $l_0 \gg R_1$ and $l_0 \ll R_1$, respectively.²⁴ We will first consider the low-speed regime, as it is the relevant one in practice. In this speed range, we have $\alpha \simeq 1 - i/(\mu_{rel}^{-1}l_0k)$, so that $\alpha kR_1 \simeq kR_1 - i(R_1/\mu_{rel}^{-1}l_0)$, and similarly for αkR_2 . Thus the imaginary part of the argument of various modified Bessel functions is much smaller than the corresponding real part. This would in turn imply that, to the leading order, the imaginary part of those functions is linear in R_1/l_0 and R_2/l_0 . This fact implies the same for Q , to wit, that in the low-speed regime the imaginary part of Q is linear in R_1/l_0 (and R_2/l_0), hence proportional to σv .²⁵ This confirms the expectation that in the low-speed regime where $l_0 \gg R_1$, the braking force is a linear drag proportional to the conductivity of the pipe wall.

The linear nature of the drag force in the low-speed regime is in evidence for all cases in Fig. 1. In typical demonstration setups, one would expect terminal speeds of the order of 1 m s^{-1} or less, which corresponds to the neighborhood of the origin in Fig. 1 where the drag force is closely proportional to the magnet speed. Indeed from the the low-speed condition $\mu\sigma v R_1 \ll 1$ given above, we can estimate the relative deviation from linearity to be of the order of $(\mu\sigma v R_1)^2$. For case (d) of Fig. 1, this estimate of deviation gives $(0.63v[\text{m s}^{-1}])^2$, which amounts to about 2.5% at a terminal speed of 25 m s^{-1} .

In the high-speed regime (which would require the projection of the magnet into the pipe with a suitably high initial speed) where $l_0 \ll R_1$, we have $\alpha \simeq (1 - i)/(2\mu_{rel}^{-1}l_0k)^{\frac{1}{2}}$ for values of $kR_1 \approx 1$ which provide the main contribution to the integral in Eq. (29). This implies that $\alpha kR_1 \simeq (1 - i)(kR_1/2)^{\frac{1}{2}}(R_1/\mu_{rel}^{-1}l_0)^{\frac{1}{2}}$, and similarly for αkR_2 . Since $R_1/l_0, R_2/l_0 \gg 1$ in this speed range, the arguments of the modified Bessel functions in Q which involve α will scale as $(R_1/l_0)^{\frac{1}{2}}$ or $(R_2/l_0)^{\frac{1}{2}}$ for $kR_1 \approx 1$. Since these functions behave exponentially for large values of their argument, the said scaling behavior results in an overall suppression $\text{Im}(Q)$ in the high speed regime, corresponding to a decrease in the drag force. In other words, the drag force is a decreasing function of σv in the high-speed regime. Physically, a pronounced skin effect which suppresses the penetration of the field into the pipe wall takes hold at high speeds, thereby reducing the eddy currents and the drag force resulting from them. Indeed, recalling from Sec. 1B that the dominant time scale in the magnet-pipe system is R_1/v , which corresponds to a frequency $\omega \approx v/R_1$, we see that the high speed condition $l_0 \ll R_1$ is equivalent to the inequality $(\mu\sigma\omega)^{-\frac{1}{2}} \ll R_1$.²⁴ But this last condition states that the skin depth corresponding to the dominant time scale is much smaller than R_1 and, barring unusually thin-walled pipes, much smaller than $R_2 - R_1$ as well. In other words, we have $(\mu\sigma\omega)^{-\frac{1}{2}} \ll R_2 - R_1$ in this limit, which is the condition for a pronounced skin effect.⁶ It is appropriate to repeat here that the high speed limit is not likely to occur in typical arrangements of the magnet-pipe demonstration.

The nonlinear behavior of the drag force at intermediate speeds and its eventual drop at high speeds deduced above are clearly in evidence for all cases displayed in Fig. 1. Note that the high-speed decline in the drag force becomes sharper as the source currents in the magnet are more highly concentrated. Recalling our discussion of the singular geometry above, we see the reason for this behavior: as source currents become more concentrated, short-distance, equivalently high- k , contributions become more important, a feature that runs contrary to the high-speed situation where high k values are relatively less important.

3. Dependence on Conductivity and Susceptibility

Recall that the drag force dependence on the magnet speed is through the combination $\mu\sigma v$. This implies that the drag force behavior versus σ follows the same pattern as for v . In particular, higher conductivity makes for a larger drag force at low speeds hence the use of copper tubes for demonstration purposes. At high speeds, however, the drag force decreases with pipe conductivity, just as it does with magnet speed. An interesting conclusion, therefore, is that the drag force vanishes for a perfect conductor which, as explained above, is simply a consequence of a strong skin effect. This behavior is displayed in Fig. 2 which is a plot of the drag force versus σ for case (d) of Sec. V A 1 at a magnet speed of 0.10 m s^{-1} . It is important to note that the decline of the drag force for high values of σ is not directly applicable to practical arrangements which usually correspond to the low-speed (or possibly intermediate-speed) regime. Also to be noted is the fact that the designation “perfect conductor” here implies electric conduction without resistance, and is to be distinguished from “superconductor” which in addition implies a distinct magnetic behavior as noted below. Of course inasmuch as a superconductor has zero resistance, the above argument shows that

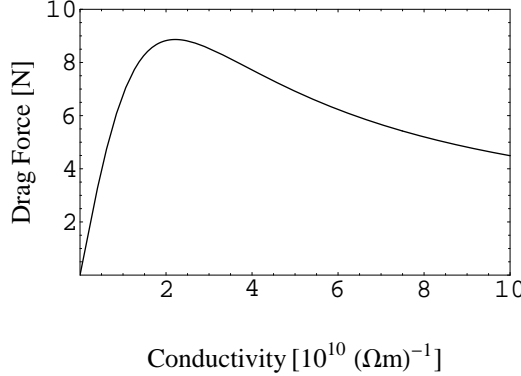


FIG. 2: Plot of the drag force versus the conductivity of the pipe for case (d) with $v = 0.10 \text{ m s}^{-1}$

the magnetic drag force vanishes for a superconducting pipe. Needless to say, this conclusion as well as the one above for a perfect conductor, directly follow from the energy conservation principle, which in this case asserts that there can be no drag force without a corresponding dissipation of power in the pipe.

This brings us to the question of how the magnetic properties of the pipe wall affect the drag force. Thus far we have assumed a linear magnetic material of relative permeability μ_{rel} for the pipe wall. Inasmuch as the magnetic susceptibility of non-ferromagnetic common metals differs little from that of the vacuum, one can set $\mu_{rel} \simeq 1$ for practical purposes, as we did for the cases displayed in Fig. 1. However, it is physically interesting and meaningful to consider the extreme cases of $\mu_{rel} \rightarrow 0$ and $\mu_{rel} \rightarrow \infty$, corresponding to perfect diamagnetism and perfect paramagnetism, respectively. Perfect diamagnetic behavior is exemplified by a (type I) superconductor which would exclude any magnetic field from its interior (save for a very small penetration depth). This phenomenon, known as the Meissner effect, is not a mere consequence of perfect conductivity and serves to distinguish a superconductor from a material that conducts electricity without dissipation.²⁶ Perfect paramagnetism, on the other hand, is approximately realized by “soft” ferromagnetic materials which have a narrow hysteresis loop and can be idealized as highly susceptible, linear magnetic materials.

An inspection of Eq. (29) shows that relative permeability occurs in the quantities α and $\beta = \alpha/\mu_{rel}$ through the combination $\mu_{rel}\mu_0\sigma v$ in α , and in addition, β is inversely proportional to μ_{rel} . Leaving the latter aside for the moment, we conclude that the drag force dependence on μ_{rel} is much like its dependence on the magnet speed. Thus the drag force must vanish for both $\mu_{rel} \rightarrow 0$ and $\mu_{rel} \rightarrow \infty$, corresponding to strongly diamagnetic and paramagnetic limits. As further discussed in Sec. V B 4, the additional dependence of β on μ_{rel} does not change these qualitative features. Thus the drag force corresponding to a superconductor vanishes not only because of its perfect conductivity but also due to its perfect diamagnetism. Similarly, the drag force is seen to be small for a strongly paramagnetic conductor, or soft ferromagnetic alloys that behave like one. The asymptotic behavior of the drag force for $\mu_{rel} \ll 1$ and $\mu_{rel} \gg 1$ is analyzed in sections V B 4 and V B 5, respectively, where the foregoing conclusions are explicitly confirmed.

Figure 3 shows a plot of the drag force versus μ_{rel} for case (d) of Sec. V A 1 at a magnet speed of 1.0 m s^{-1} , where the features deduced above are in evidence.

B. Asymptotic Behavior

In this section we will outline the development of a few limiting expressions for the drag force given in Eq. (29). The methods used are those of approximation and asymptotic analysis of integrals the details of which would take us beyond the scope of this paper.²⁷

As a preliminary step we recall that in all cases except for Sec. V B 4 the main contributions to the integral of Eq. (29) originate in the region $k \simeq R_1^{-1}$. This fact makes it convenient to rescale the integration variable therein according to $k = u/R_1$. Effecting this substitution, we obtain

$$\mathbf{F} = -\hat{\mathbf{v}} \frac{\mu_0 m^2}{2\pi^2 R_1^4} \int_0^{+\infty} du u^3 \left[\frac{\sin(uL/2R_1)}{(uL/2R_1)} \right]^2 \left[\frac{I_1(ua/R_1)}{(ua/2R_1)} \right]^2 \text{Im}[Q(u, s/R_1, R_1/l_0, \mu_{rel})], \quad (33)$$

where we have explicitly defined the dependence of Q on three dimensionless parameters which characterize the

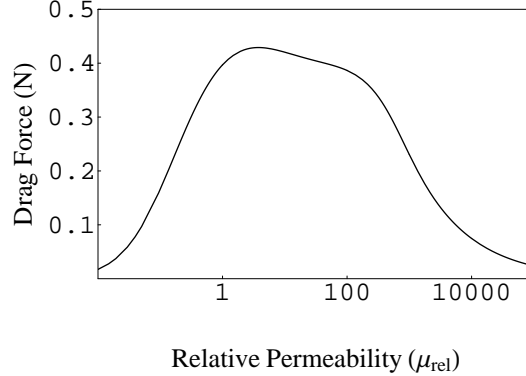


FIG. 3: Plot of the drag force versus the relative permeability of the pipe for case (d) with $v = 1.0 \text{ m s}^{-1}$

dimensions and material properties of the pipe as well as the magnet speed. We shall use this representation to derive asymptotic expressions for the drag force in a number of interesting limiting cases.

1. Low Magnet Speed

The low-speed regime is defined by the condition $R_1/l_0 \ll 1$.²⁴ To establish the fact that \mathbf{F} is linear in v in the low-speed limit, as discussed in Sec. V A 2, we note that $Q(u, s/R_1, 0, \mu_{rel})$ is real at $v = 0$ (corresponding to the vanishing of the drag force at zero speed), so that an expansion of $\text{Im}(Q)$ about $v = 0$ using the asymptotic properties of the modified Bessel functions¹⁸ yields $\text{Im}[Q(u, s/R_1, R_1/l_0, \mu_{rel})] \cong \mathcal{L}R_1/l_0$ for small R_1/l_0 . The quantity \mathcal{L} equals $\text{Im}[\partial Q(u, s/R_1, 0, \mu_{rel})/\partial(R_1/l_0)]$, and is given by a long expression which need not be reproduced here. Substituting the approximate form of $\text{Im}(Q)$ in Eq. (33), we immediately obtain the linear drag behavior in the low-speed limit:

$$\mathbf{F}^{lsp} \cong -\mathcal{C}\sigma v \hat{\mathbf{v}} \quad (\mu_{rel}\mu_0\sigma v R_1 \ll 1), \quad (34)$$

where \mathcal{C} depends on all parameters other than σ and v .

2. The Idealized Model

The idealized model involves three assumptions, (a) the point-dipole limit, $L/R_1 \rightarrow 0$, $a/R_1 \rightarrow 0$, (b) the low-speed approximation, $R_1/l_0 \ll 1$, and (c) the thin-wall approximation, $s/R_1 \ll 1$. The point-dipole limit is readily implemented by setting the two shape factors equal to unity. Items (b) and (c), on the other hand, require applying the thin-wall approximation to the quantity \mathcal{C} introduced in Eq. (34). Using the properties of the modified Bessel functions, we find from Eqs. (23-25) that $\mathcal{C} \rightarrow (s/R_1)u[K_1(u)]^2$. Therefore,

$$Q^{idl} = i\mu_0(s/R_1)u[K_1(u)]^2\sigma v, \quad (35)$$

where Q^{idl} represents Q in the ideal limit. Substituting this result in Eq. (33) (with the shape factors set to unity), we find

$$\mathbf{F}^{idl} = -\frac{45\mu_0^2 m^2 s}{1024 R_1^4} \sigma v \hat{\mathbf{v}}, \quad (36)$$

in agreement with previous results.²

3. High Magnet Speed

As stated in Sec. V A 2, in the high-speed regime where $l_0/R_1 \ll 1$, the quantity α in Eqs. (23-25) has a large magnitude which forces the respective modified Bessel functions to their asymptotic range. Since the four quantities

T_{ij} in Eqs. (24) have the same asymptotic limit,¹⁸ they cancel out of Eq. (23). The remaining terms can then be simplified using the properties of the modified Bessel functions, leaving the result

$$\text{Im}(Q) \cong \frac{1}{kR_1} \frac{-\text{Im}(\beta)}{[I_0(|k|R_1)]^2 + |\beta|^2 [I_1(|k|R_1)]^2} \quad (\mu_{\text{rel}}\mu_0\sigma v \gg R_1). \quad (37)$$

The remaining v dependence in Eq. 37 resides in $\beta = \alpha/\mu_{\text{rel}}$. Recalling from Sec. V A 2 that $\alpha \rightarrow (1-i)/(2\mu_{\text{rel}}^{-1}l_0k)^{\frac{1}{2}}$ in the high-speed limit, we can reduce the above equation to²⁴

$$\begin{aligned} \text{Im}(Q) &\cong \frac{\sqrt{\mu_{\text{rel}}}}{\sqrt{2k\mu_0\sigma v}R_1[I_1(|k|R_1)]^2} \\ &= \frac{\sqrt{\mu_{\text{rel}}}}{\sqrt{2uR_1/l_0[I_1(u)]^2}} \quad (\mu_{\text{rel}}\mu_0\sigma v \gg R_1). \end{aligned} \quad (38)$$

Upon substituting this expression in Eq. 33, we find

$$\mathbf{F}^{hsp} = -\frac{0.274m^2}{R_1^{9/2}} \mathcal{F}_1(a/R_1, L/R_1) \sqrt{\frac{\mu}{\sigma v}} \hat{\mathbf{v}}, \quad (39)$$

where \mathcal{F}_1 is a form factor which depends on the dimensions of the magnet as fractions of the interior diameter of the pipe. It is defined by

$$\mathcal{F}_1(a/R_1, L/R_1) = \frac{\mathcal{G}_1(a/R_1, L/R_1)}{\mathcal{G}_1(0, 0)}, \quad (40)$$

where

$$\mathcal{G}_1(a/R_1, L/R_1) = \int_0^{+\infty} du u^{5/2} \left[\frac{\sin(uL/2R_1)}{(uL/2R_1)} \right]^2 \left[\frac{I_1(ua/R_1)}{(ua/2R_1)} \right]^2 [I_1(u)]^{-2}. \quad (41)$$

Note that the form factor \mathcal{F}_1 has been normalized to unity at the point-dipole limit.

The asymptotic formula in Eq. (39) is valid in the high-speed limit $\mu_{\text{rel}}\mu_0\sigma v \gg R_1$ and describes the behavior of the drag force for very high magnet speed or pipe wall conductivity.²⁴

4. Highly Diamagnetic Pipe

This is the limit $\mu_{\text{rel}} \rightarrow 0$, which is appropriate to a highly diamagnetic pipe wall material. In this limit the factor β which occurs in Q grows large and severely suppresses the magnitude of $\text{Im}(Q)$ in Eq. (33), and in addition limits its contributions to very small values of u . This mathematical behavior reflects the physical phenomenon of magnetic flux expulsion that accompanies the approach to perfect diamagnetism.

Since only small values of u are important in Eq. (33), we can replace all modified Bessel functions by their asymptotic values in the small argument limit.¹⁸ This leads to the following approximate expression for Q :

$$Q = -\frac{\alpha^2 \ln(R_2/R_1)}{\mu_{\text{rel}} + \frac{1}{2}u^2 \ln(R_2/R_1)\alpha^2}. \quad (u \ll 1) \quad (42)$$

Next, we find $\text{Im}(Q)$ and change the variable of integration in Eq. (33) according to $w = \mu_{\text{rel}}^{-\frac{1}{2}} \ln(R_2/R_1)^{\frac{1}{2}} u$. After some calculation and simplification, we find

$$\mathbf{F}^{hdm} = -\mathcal{K} \int_0^{+\infty} d\zeta \zeta^2 \left[1 + \frac{1}{2}\zeta^2 \right]^{-2} \hat{\mathbf{v}}, \quad (43)$$

where

$$\mathcal{K} = \frac{\mu_0^2 m^2 \sigma v}{2\pi^2 R_1^3} [\ln(R_2/R_1)]^{-\frac{1}{2}} \mu_{\text{rel}}^{3/2}. \quad (44)$$

Finally, we carry out the integral in Eq. (43) to arrive at the asymptotic behavior of the drag force:

$$\mathbf{F}^{hdm} = -\frac{\mu_0^2 m^2 \sigma v}{2\pi\sqrt{2}R_1^3} [\ln(R_2/R_1)]^{-\frac{1}{2}} \mu_{\text{rel}}^{3/2} \hat{\mathbf{v}}. \quad (45)$$

The above formula is valid in the limit $\mu_{\text{rel}} \rightarrow 0$, and is appropriate to a highly diamagnetic pipe.

5. Highly Paramagnetic Pipe

Here we are considering the limit $\mu_{rel} \rightarrow \infty$ appropriate to a highly susceptible pipe wall material. Recall from [VA3](#) that the dependence of Q on μ_{rel} occurs through the combination $\mu_{rel}\mu_0\sigma v$ in α , and in addition through $\beta = \alpha/\mu_{rel}$. Consequently, Eq. [37](#) which is appropriate in the high-speed regime holds here as well. Recalling further that $\beta \rightarrow (1-i)/(2\mu_{rel}l_0k)^{\frac{1}{2}}$ in this limit, we find

$$\text{Im}(Q) \cong \frac{1}{\sqrt{2u^3l_0/R_1[I_0(u)]^2\sqrt{\mu_{rel}}}} \quad (\mu_{rel} \gg 1). \quad (46)$$

At this point we follow the steps subsequent to Eq. [37](#) to find

$$\mathbf{F}^{hpm} = -\frac{0.0536\mu_0^2m^2}{R_1^{7/2}}\mathcal{F}_0(a/R_1, L/R_1)\sqrt{\frac{\sigma v}{\mu}}\hat{\mathbf{v}}, \quad (47)$$

where \mathcal{F}_0 is a form factor which depends on the dimensions of the magnet as fractions of the interior diameter of the pipe. It is defined by

$$\mathcal{F}_0(a/R_1, L/R_1) = \frac{\mathcal{G}_0(a/R_1, L/R_1)}{\mathcal{G}_0(0, 0)}, \quad (48)$$

where

$$\mathcal{G}_0(a/R_1, L/R_1) = \int_0^{+\infty} du u^{3/2} \left[\frac{\sin(uL/2R_1)}{(uL/2R_1)} \right]^2 \left[\frac{I_1(ua/2R_1)}{(ua/2R_1)} \right]^2 [I_0(u)]^{-2}. \quad (49)$$

Note that the form factor \mathcal{F}_0 has been normalized to unity at the point-dipole limit.

The asymptotic formula given in Eq. [\(46\)](#) is valid in the limit $\mu_{rel} \gg 1$ and describes the behavior of the drag force for a highly susceptible pipe.

VI. CONCLUDING REMARKS

In this paper we have explored the physics of magnetic braking in the context of the demonstration involving a magnet falling inside a conducting pipe. Our primary objectives were (a) to develop a reasonably realistic, quantitatively useful, and analytically manageable formulation of the magnet-pipe system, and (b) to discuss as completely as practicable the physical phenomena relevant to the magnet-pipe system. We believe these objectives have been realized as evidenced by, e.g., the results presented in Sec. [V](#). We have also considered several extensions of the basic experiment where conditions well beyond those of a typical demonstration arrangement have been treated.

The present formulation can be readily extended to the case of a permanent magnet possessing a nonuniform, azimuthally symmetric magnetization with components in the radial and axial directions. Commercially available magnets are likely to deviate from the uniform, axial magnetization assumed here. If sizable, such a deviation can become a source of significant error. Although a sufficiently accurate characterization of the magnetization distribution can be a nontrivial experimental task, it might be unavoidable if a close quantitative agreement with measured results is desired.

The extension to nonuniform magnetization mentioned above is conceptually straightforward. This is because, with the magnetization geometry stipulated above, the bound source currents will amount to an azimuthally symmetric distribution of current rings. The fields corresponding to such a distribution will then be given by a superposition of those arising from a corresponding distribution of single current rings.²⁸ Indeed the fields constructed in Sec. [III](#) are just such a superposition corresponding to bound current rings circulating at the surface of the magnet. Thus the extension to nonuniform magnetization merely amounts to a more general superposition where the source current rings are distributed over the volume of the magnet as well as its surface. This generalization will be reflected in Eq. [\(8\)](#) which will be extended to a double integral, and similarly for the integral of Eq. [\(29\)](#) which defines the drag force.

The treatment of the magnet-pipe system in this paper has been based on azimuthal symmetry. Therefore, any deviation of the magnet from a linear, axially centered motion such as wobbling or tumbling would violate this underlying assumption and cause a departure from the predicted results. It is therefore crucial to minimize any such deviation where a quantitative comparison with measured results is intended. A convenient method of achieving

this is to place the magnet inside an electromagnetically inactive casing with an optimum profile for stability. This procedure would also serve to maintain a fixed air drag coefficient when comparing magnets of different profile.

Finally, it is worth recalling that our analysis assumes an infinitely long pipe, so that in practice each magnet end is required to be many times the interior pipe diameter away from the near end of the pipe when measurements are taken.

Acknowledgments

MHP's work was supported in part by a research grant from California State University, Sacramento.

* Electronic address: hpartovi@csus.edu

† Electronic address: simplysimian@yahoo.com

¹ J. A. M. Clack and T. P. Toepker, *Phys. Teach.* **28**, 236 (1990).

² W. M. Saslow, *Am. J. Phys.* **60**, 693 (1992).

³ C. S. Maclatchy, P. Backman, and L. Bogan, *Am. J. Phys.* **61**, 1096 (1993).

⁴ K. D. Hahn, E. M. Johnson, A. Brokken, and S. Baldwin, *Am. J. Phys.* **66**, 1066 (1998).

⁵ N. Gauthier, *Am. J. Phys.* **70**, 103 (2002).

⁶ J. D. Jackson, *Classical Electrodynamics*, 3rd ed. (John Wiley, New York, 1999), pp. 218-220.

⁷ The SI system of units will be used throughout this paper.

⁸ A *Mathematica* program for computing the drag force as a function of velocity from Eq. (29) is provided for this purpose and may be downloaded from this URL: <http://www.csus.edu/indiv/p/partovimh/magpipedrag.nb>.

⁹ S. Weinberg, *Gravitation and Cosmology* (John Wiley, New York, 1972), pp. 67-70.

¹⁰ See Jackson,⁶ p. 192.

¹¹ *Ibid.*, p. 554 *et seq.*

¹² D. J. Griffiths, *Introduction to Electrodynamics* (Prentice Hall, New Jersey, 1999), third ed., p. 531.

¹³ Recall the discussion in the Sec. 1B concerning the quasi-static limit.

¹⁴ See Jackson,⁶ p. 126.

¹⁵ *Ibid.*, Chapter 9.

¹⁶ The dipole radiation can be found from the magnetic dipole radiation formula, $(\mu_0/6\pi c^3)\dot{M}^2$, where \mathbf{M} is the dipole moment in question. Using this formula, and recalling that the magnet's dipole moment in the laboratory frame equals m/γ , we find the result $(\mu_0 m^2/6\pi c^7)(\dot{v}^2 + v\ddot{v})^2$. This quantity is in general smaller than the quadrupole radiation by a factor of order $(v/c)^2$.

¹⁷ There is a zeroth region, (0), defined by $0 \leq \rho \leq a$, which we have not included here. The potential in this region is obtained from that in region (i) by substituting the appropriate representation of $\tilde{A}^{(i)}(\rho, k)$ valid for $0 \leq \rho \leq a$. The latter is defined in the paragraph following Eq. (7).

¹⁸ G. B. Arfken and H. J. Weber, *Mathematical Methods for Physicists*, 5th ed. (Academic Press, San Diego, CA, 2001), Chapter 11.

¹⁹ The imaginary part of Q is positive, a fact that is not readily obvious from its definition.

²⁰ An analogous situation obtains for the electrostatic force exerted on a charged object by its image with respect to a conducting or (linear) dielectric medium. Such a force would scale with the square of the real charge.

²¹ In effect the thin-wall approximation assumes uniform fields and eddy currents within the pipe wall thus ignoring the inevitable fall-off of all disturbances away from the axis. This is the reason why the thin-wall approximation in general overestimates the drag force.

²² Air drag effects can of course be eliminated by placing the pipe-magnet system in an evacuated chamber.

²³ Recall that we have already restricted v to nonrelativistic values.

²⁴ Here we are implicitly assuming that μ_{rel} is of the order of unity. We will consider departures from this assumption in V A 3, and more specifically, the possibilites of $\mu_{rel} \ll 1$ and $\mu_{rel} \gg 1$ in sections V B 4 and V B 5, respectively.

²⁵ Because the dependence of Q on μ is not just through the Bessel functions, this argument fails to give the full dependence of the force on μ .

²⁶ N. W. Ashcroft and N. D. Mermin, *Solid State Physics* ((Holt, Rinehart, and Winston, New York, 1976), p. 731.

²⁷ A general reference for asymptotic analysis is Norman Bleistein and Richard A. Handelsman, *Asymptotic Expansions of Integrals* (Dover Publications, New York, 1986); see also the textbook by Arfken and Weber¹⁸.

²⁸ This is essentially the method of Green's function for solving boundary value problems associated with linear systems; see, e.g., the textbook by Arfken and Weber,¹⁸ or Jackson,⁶ for a detailed description of this method.